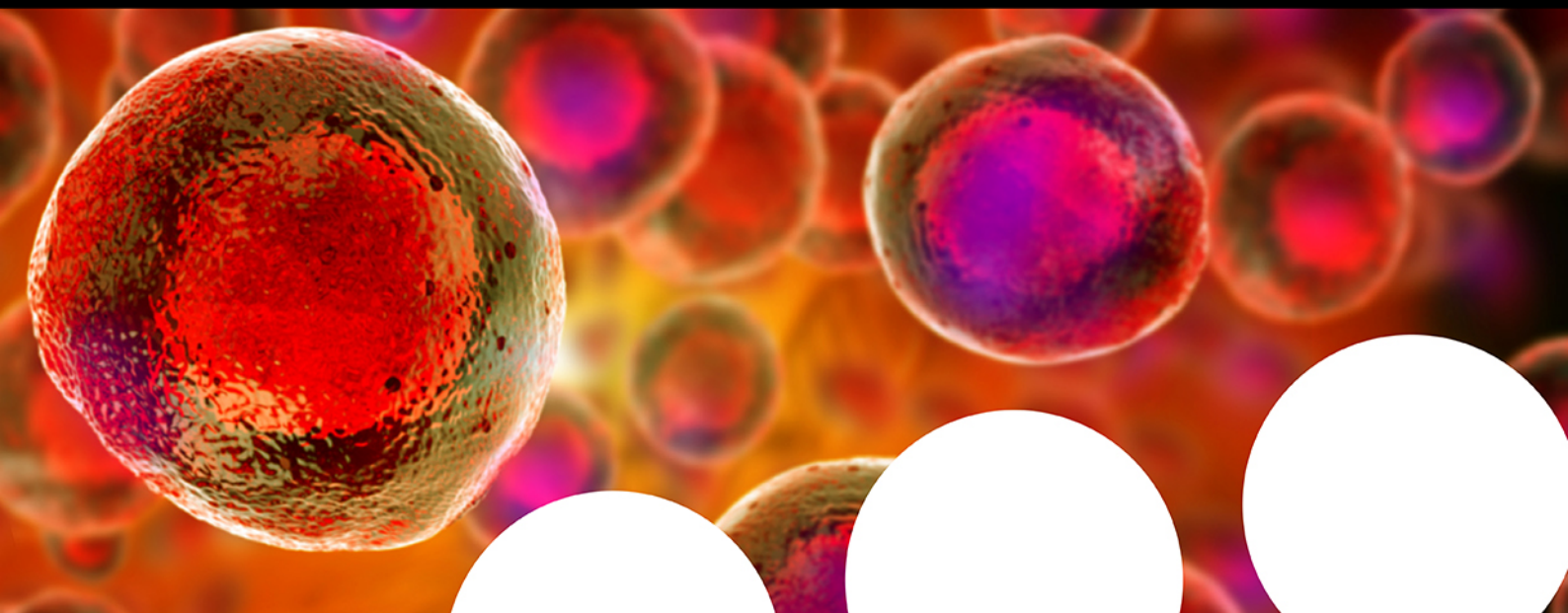


Your research is important and needs to be shared with the world



Benefit from the Chemistry Europe Open Access Advantage

- Articles published open access have higher readership
- Articles are cited more often than comparable subscription-based articles
- All articles freely available to read, download and share.

Submit your paper today.



www.chemistry-europe.org

Special
Collection

Oxygen-Doped PAH Electrochromes: Difurano, Dipyrano, and Furano-Pyrano Containing Naphthalene-Cored Molecules

Jack Fletcher-Charles,^[a] Rúben R. Ferreira,^[b] Michael Abraham,^[b] Deborah Romito,^[b] Markus Oppel,^[c] Leticia González,^[c] and Davide Bonifazi*^[a, b]*In memory of François Diederich*

In this work, we report the synthesis of O-doped naphthalene-based electrochromes. Exploiting the CuO-mediated Pummerer oxidative cycloetherification reaction, a series of 1,4- and 1,5-disubstituted naphthalene-cored dipyrano, difurano, and furano-pyrano polycyclic aromatic hydrocarbons (PAHs) have been prepared. Steady-state UV-Vis absorption and emission investigations showed that the spectroscopic profile strongly depends on the O-doping topology, with the dipyrano and the difurano derivatives demonstrating the most red-shifted and

blue-shifted electronic transition, respectively. Computational investigations revealed that the cycloetherification reaction raises the HOMO energy level (while the LUMO remains largely unaffected), with the dipyrano derivatives displaying the highest values. Spectroelectrochemical measurements showed that, depending on the O-topology and the type of O-ring, different electrochromic responses could be obtained with colour transitions featuring high contrasts involving yellow, pink, orange or blue colours.

Introduction

In recent years, electrochromism has garnered considerable interest as a low-energy visualisation technology which could be used in flexible electrochromic displays (ECDs),^[1–5] smart windows,^[6–9] self-dimming rear-view mirrors,^[10] and wearable tech.^[11–14] Electrochromism, as a general definition, is the ability of a material to reversibly change colour upon the application of an electric current.^[15,16] One of the first documented examples, and one that is often purported as the beginning of the field, is the work from Deb et al. who found that WO₃ could

be oxidised in acidic media from colourless to deep blue.^[17] Much of the early work in this field focussed on metal oxides and complexes such as WO₃,^[18–20] NiO,^[21–24] and Prussian blue,^[25–28] however, work quickly moved on to using organic architectures (e.g., polymers and small molecules, see below) as electrochromic units, *i.e.* electrochromes. This is in part due to several advantages that organic electrochromic structures have over their metal oxide counterparts: they can be printed on flexible substrates for engineering flexible devices,^[29–35] they provide greater processability to allow for deposition techniques such as inkjet printing to be used,^[36,37] and the colour changes can be tuned through classical organic synthetic means by specific lateral functionalisation of the π -conjugated framework.^[38–43]

Organic electrochromes can be split into two families: polymeric and small molecule electrochromes.^[15,44–46] The majority of research conducted in this area has taken advantage of polymeric materials, in particular polythiophenes have been the focus of many researchers.^[28,47–50] Electrochromic polymers such as PEDOT, PEDOP, PProDOP, P3MT, and their derivatives, have greatly furthered the research into the topic of electrochromism, providing materials with fast switching times (< 1 s), high contrasts (up to 89 $\Delta\%$ T), and good cyclability (> 5000 ON/OFF cycles).^[51–55]

However, polymeric electrochromes have not been alone in garnering interest; the most prominent real-world application of ECDs (self-dimming rear-view mirrors) actually utilises a viologen derivative as its electrochromic component.^[56–59] Electrochromic viologens have been thoroughly investigated by many groups, producing a wide variety of derivatives through extension of the aromatic core or variation of the chemical nature of the *N*-substituents.^[59–63] They have, however, shown limited scope in applications as they tend to adopt only blue or

[a] J. Fletcher-Charles, Prof. Dr. D. Bonifazi
School of Chemistry,
Cardiff University
Cardiff, CF10 3AT, United Kingdom

[b] R. R. Ferreira, M. Abraham, D. Romito, Prof. Dr. D. Bonifazi
Institute of Organic Chemistry,
Faculty of Chemistry,
University of Vienna
1090 Vienna, Austria
E-mail: davide.bonifazi@univie.ac.at
<https://bonifazi-group.univie.ac.at>

[c] Dr. M. Oppel, Prof. Dr. L. González
Institute of Theoretical Chemistry,
Faculty of Chemistry,
University of Vienna
1090 Vienna, Austria

Supporting information for this article is available on the WWW under <https://doi.org/10.1002/ejoc.202101166>

This article belongs to a Joint Special Collection dedicated to François Diederich.

© 2021 The Authors. European Journal of Organic Chemistry published by Wiley-VCH GmbH. This is an open access article under the terms of the Creative Commons Attribution Non-Commercial NoDerivs License, which permits use and distribution in any medium, provided the original work is properly cited, the use is non-commercial and no modifications or adaptations are made.

purple colours in their coloured state. The field has now begun looking to other types of organic molecules in an attempt to obtain electrochromic materials featuring a vast array of different colourless-to-coloured transitions in the visible spectrum. The main challenges in the field are to obtain colourless-to-red, colourless-to-yellow and colourless-to-green electrochromic transitions.

Recent work has demonstrated that other well-known, readily accessible, all-carbon polycyclic aromatic hydrocarbons (PAHs) also possess electrochromic properties. For instance, anthracene and perylene have both been integrated into prototype devices although requiring high operating potentials to achieve a colour change (from -4 to 4 V).^[64,65]

Taking advantage of their low oxidation potentials, O-doped PAHs can be considered as one of the promising classes of electrochromic small molecules. Amongst all O-doped molecules,^[66] those featuring furanyl,^[67–71] pyranyl,^[72–74] or oxepinyl^[75,76] rings are of particular interest to the area of optoelectronics,^[66] especially as *p*-type semiconductors.^[67] One of the most well-known examples of an O-doped electrochrome can be found in the *peri*-xanthenoxanthene (PXX, Figure 1),^[77,78] a well-known molecular *p*-type semiconductor that was one of the first pyranyl-conjugates to exhibit electrochromic properties (from yellow to blue).^[79,80]

Recently, our group has gone on to expand the library of O-doped PAHs through the development of Cu-catalysed intramolecular etherification reactions.^[81–86] For instance, we have demonstrated that smaller O-doped molecules containing furanyl, pyranyl, and oxepinyl moieties could be easily accessed through CuO-mediated Pummerer-type oxidative cyclisation.^[87] In these works, it has been shown that the formation of pyrano rings provokes a rise of the HOMO energy level, which results in a shrinking of the HOMO-LUMO gap and in the lowering of the oxidation potential.^[82]

Considering that colourless materials can be obtained with PAHs displaying limited conjugation and that the introduction of O-atoms in the all-carbon framework improves the *p*-type

semiconducting properties, in this work we planned to prepare colourless O-doped PAHs featuring limited π -conjugation (1,4-dipyrano and 1,5-dipyrano, Scheme 1).^[81,82] Upon oxidation, an increase of the π -conjugation within the molecule is expected to occur due to the antiaromatic to aromatic transition of the pyrano moieties, thus leading to a coloured state.

Building on the Cu-mediated oxidative etherification reaction,^[83,87] we proposed the preparation of O-doped PAHs in which pyrano rings are developed from a naphthyl core (Scheme 1). In particular we planned two isomeric structural motifs: *cisoid* and *transoid* dipyrano derivatives to study the effect of the positional doping on the molecular electrochromic properties. We envisioned these PAHs as arising through cross coupling reaction of a hydroxy-bearing aryl boronic acid with either 1,4- or 1,5-dibromo naphthalene derivatives followed by the C–O oxidative cyclisation reaction occurring at the free naphthyl *peri*-positions. Upon synthesis of the desired pyrano-containing molecules, we aim to fully characterise them with regards to the change in their optical properties upon oxidation through spectroelectrochemical investigations. Special attention will be paid to the electrochemical properties, focussing on those derivatives depicting oxidation potentials falling within the operating potential of a typical ECD (1–2 V).

Results and Discussion

Synthesis and Structural Characterisation

Synthetic attempts started on the preparation of 1,4-disubstituted naphthalenyl precursors (molecule 4, Scheme 2) with initial work unsuccessfully following a synthetic strategy which pursued the addition of an aryllithium nucleophile to commercially available 1,4-naphthoquinone. The first steps of this path involved the bromination of 3-*tert*-butylphenol (91%), followed by the methylation of the hydroxyl group to give molecule 1 (Scheme 2). Li-halogen exchange using molecule 1 and addition of the resulting organolithium derivative to a solution of 1,4-naphthoquinone gave none of the desired hydroxy-bearing precursors. Further work instead utilised a one-pot nucleophilic addition followed by the reduction of the diol. While the desired product 4 was isolated in poor yield (13%), naphthalenol 3 was obtained in 77% yield (Scheme 2). Following on from this initial attempt, the synthetic strategy was adjusted to bypass the troublesome nucleophilic addition to naphthoquinone step. Instead, it was decided that a Pd-catalysed cross-

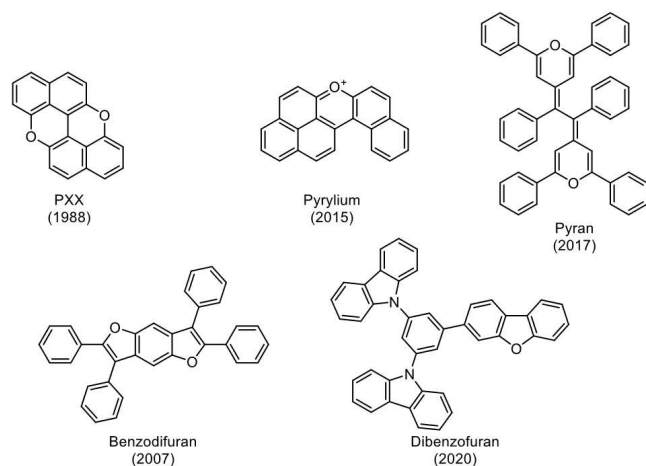
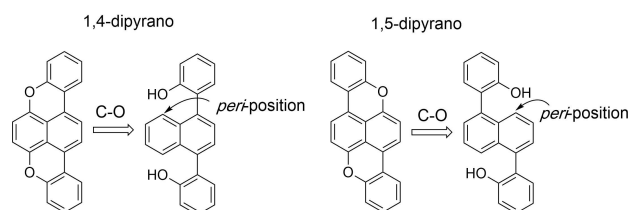
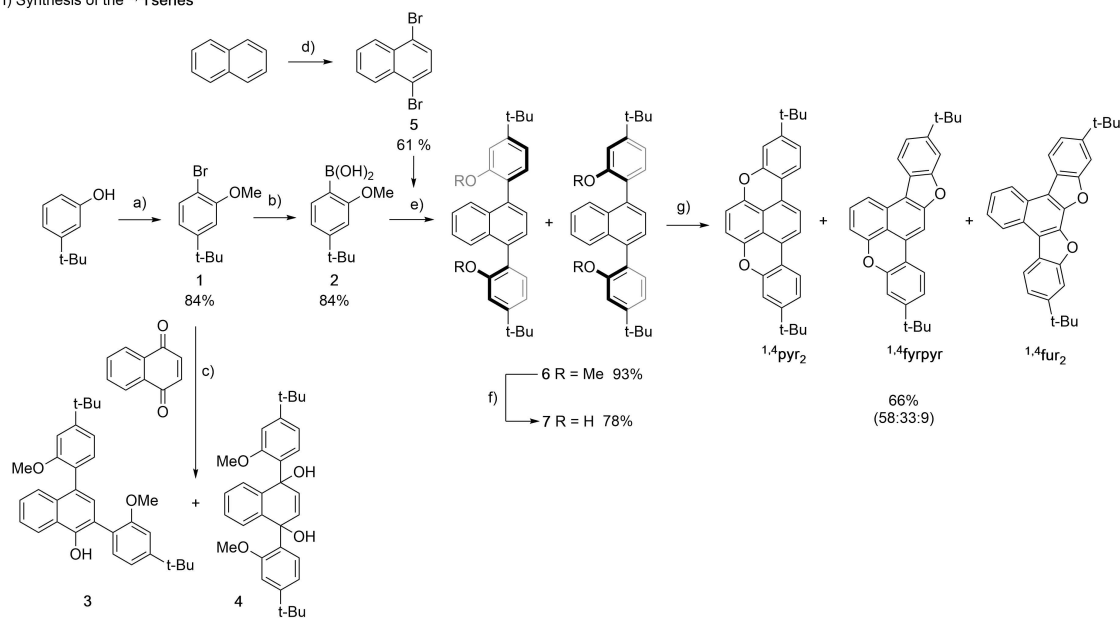


Figure 1. Five notable examples of O-doped PAHs that have found application in the area of organic electronics as both semiconductors and electrochromes.^[69,72,73,79]

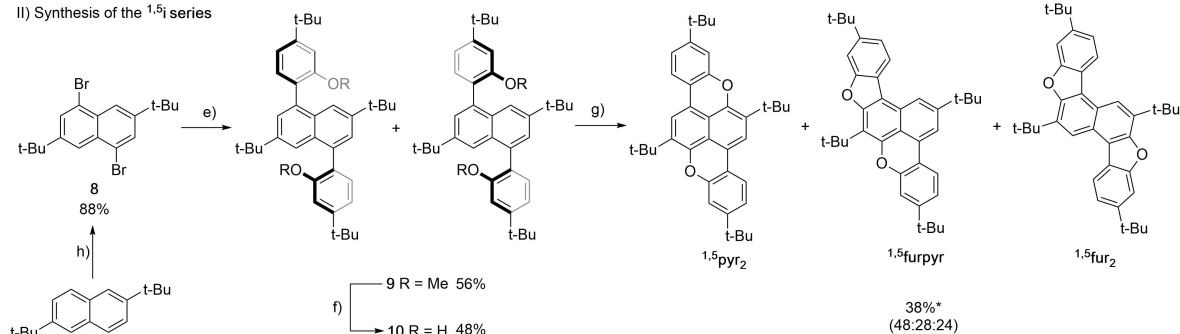


Scheme 1. Targeted O-doped PAHs featuring dipyranyl rings developing from 1,4- and 1,5-disubstituted naphthalene cores.

I) Synthesis of the ^{1,4}i series



II) Synthesis of the ^{1,5}i series



Scheme 2. The synthetic routes towards O-doped naphthalenyl molecular derivatives ^{1,4}i series and ^{1,5}i series. Reagents and conditions: a) 1. Br₂, CH₂Cl₂, 0 °C. 2. CH₃I, K₂CO₃, DMF, 55 °C; b) 1. *n*-BuLi, B(OMe)₃, THF, −84 °C to r.t. 2. 1 M HCl_(aq), r.t.; c) 1. *n*-BuLi, Et₂O, −78 °C. 2. 1,4-naphthoquinone, Et₂O, r.t. 3. SnCl₂ in conc. HCl at r.t.; d) Br₂, CH₂Cl₂, −35 °C to 10 °C; e) K₂CO₃, [Pd(PPh₃)₄], Dioxane/H₂O, 85 °C; f) BBr₃, CH₂Cl₂, −84 °C to r.t.; g) CuO, PhNO₂, reflux; h) AlCl₃, Br₂, CH₂Cl₂, −10 °C to r.t. *This yield does not include the dealkylated O-doped species.

coupling reaction would be utilised to build the dihydroxy precursor. Following this route, boronic acid **2** was obtained through a one-pot Li-halogen exchange followed by electrophilic borylation reaction in very good yields (84%).^[81] The 1,4-dibromonaphthalene counterpart (**5**) was obtained through bromination of naphthalene, using a literature procedure^[88] and gave access to the desired product in 61% yield (Scheme 2). Suzuki cross-coupling reaction between **2** and **5** afforded desired 1,4-disubstituted naphthalene product **6** as atropisomeric mixture (i.e., *S,R* and *R,R*) in 93% yield, which then underwent a demethylation reaction following literature procedure using BBr₃. Upon obtaining the deprotected disubstituted naphthalene molecule **7** as an atropisomeric mixture (see Figures S16 for the isomerisation studies) in good yield (78%), attempts to perform the intramolecular etherification reaction using CuI and PivOH in DMSO, as developed previously by our group,^[81–83] were conducted. These initial attempts did not yield any of the desired products, with very little to no conversion seen (Scheme 2). Instead, Pummerer's protocol with CuO in

refluxing PhNO₂ was applied, leading to an isomeric mixture (in a 58:33:9 ratio) of di-O-doped PAHs in 66% yield. Purification of the mixture by recycling HPLC allowed for the separation of the isomers, affording the difurano (^{1,4}fur₂), the furano-pyrano (^{1,4}furpyr) and dipyrano (^{1,4}pyr₂) derivatives as white, yellow, and orange powders (Scheme 2).

In parallel, synthetic work aiming to obtain the analogous 1,5-dipyrano molecule (^{1,5}pyr₂) was performed. This synthesis followed a similar strategy (Scheme 2) as that applied to prepare ^{1,4}pyr₂. Bromination of 2,6-di(*tert*-butyl)naphthalene was performed according to literature procedure, with the *tert*-butyl groups being used as directing groups to selectively brominate at the 1 and 5 positions, giving access to the desired 1,5-dibrominated naphthalene core (**8**) in good yield (88%).^[89]

Molecule **8** was then reacted with **2** utilising similar Suzuki cross coupling reaction conditions as those used for preparing **6**, yielding **9** in a good amount (56%) as a mixture of atropisomers. Disubstituted naphthalene intermediate **9** was demethylated with BBr₃ to obtain diol molecule **10** as an

atropisomeric mixture (see Figure S17) in fair yield (48%). CuO-mediated ring closure in PhNO₂ yielded a mixture of O-cyclised isomers (38%) in a 48:28:24 ratio (Scheme 2). Analogously to the case of the 1,4-disubstituted naphthalene, HPLC purification led to the isolation of the difurano (^{1,5}fur₂), the furano-pyrano (^{1,5}furpyr) and the dipyrano (^{1,5}pyr₂) derivatives as white, yellow, and orange solids. Unfortunately, under these reaction conditions a considerable amount of de-*tert*-butylated products (see SI) were also isolated from purification by recycling HPLC, preventing us from precisely estimating the total yield of the ^{1,5}i series products.

Attempts to characterize the cyclised products were performed by single-crystal X-ray. Small crystals of ^{1,4}pyr₂ suitable for XRD analysis were grown by liquid diffusion of

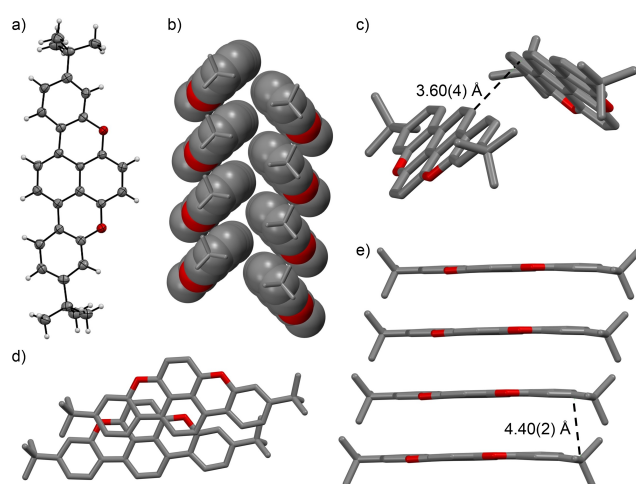


Figure 2. a) ORTEP representation (50% probability ellipsoids) of ^{1,4}pyr₂; b) space filling view of the molecular packing, c) edge-to-face and e) face-to-face interactions, distances are expressed in Å; d) detail of the offset π - π arrangement. Space group: P-1. Crystallization solvents: CH₂Cl₂/MeOH.

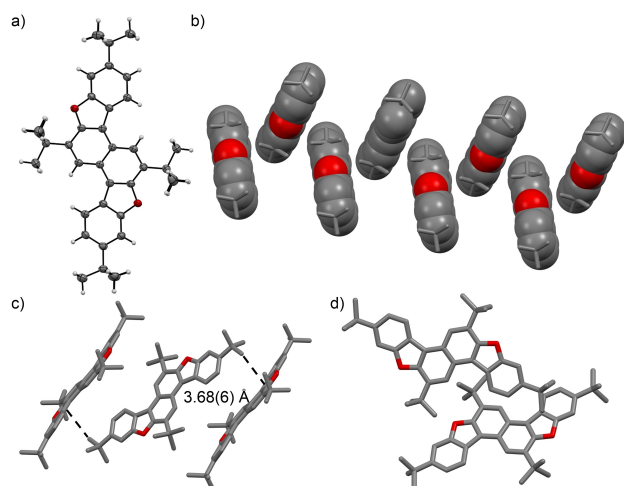


Figure 3. a) ORTEP representation (50% probability ellipsoids) of ^{1,5}fur₂; b) space filling view of the crystal structure, having a herringbone fashion and being based on c) C-H... π interactions (distances are expressed in Å); d) crystal packing front view. Space group: P2₁c. Crystallization solvents: CH₂Cl₂/MeOH.

CH₂Cl₂ in MeOH. The crystal structure of ^{1,4}pyr₂ confirms the presence of the two pyranyl rings (Figure 2a). Looking at the molecular packing, a double columnar arrangement is depicted (Figure 2b), with the molecules disposed in a herringbone fashion. Each molecule simultaneously develops an antiparallel edge-to-face interaction of 3.60(4) Å (Figure 2c), as well as a weak face-to-face π - π stacking of 4.40(2) Å (Figure 2e). Notably, the π -stacked columnar arrangement sees the molecules organised parallelly with an offset of \sim 1 Å (Figure 2d).

The molecular structure of ^{1,5}fur₂ was confirmed by XRD analysis of crystals grown through liquid-liquid diffusion using a CH₂Cl₂/MeOH mixture (Figure 3a). In this case, the molecular packing is exclusively driven by C-H... π interactions of 3.68(6) Å, involving the *t*-butyl moieties and the π -conjugated backbone of a neighbouring molecule (Figure 3c). This results in the formation of a kinked arrangement, with the molecules disposed in a herringbone motif (Figure 3b). This organization prevents the occurrence of π - π stacks since neighbouring molecules show an inclination of \sim 35° (Figure 3d). Attempts to obtain crystals with sufficient quality for X-ray diffraction for the other O-doped derivatives were unsuccessful.

In an attempt to rationalise the formation of three isomers from one reaction, we have postulated that the cyclisation reaction occurs through adsorption of the 1,4- and 1,5-substituted naphthalenyl di-hydroxy precursors onto the CuO surface, after which the ring closures can occur simultaneously in the same or opposite directions, or independently in a stepwise fashion (Figure 4 for the 1,4-naphthalenyl derivative, Figure S1 for the 1,5-naphthalenyl derivative). Excluding any atropisomeric effects deriving from the di-hydroxy precursors (the temperature of the Pummerer's reaction with CuO is well above the activation energy for the rotation around the C(Ar)-C(Naphtalene) bond, see Figures S17–S18), one can hypothesise that the di-hydroxy precursors adsorb on the surface as bidentate ligands. Building on this hypothesis, one can envisage the formation of the three isomers for the 1,4-substituted naphthalenyl precursors (Figure 4) while travelling through either the stepwise or concerted reaction mechanism. Through the simultaneous ring closure mechanism, one can envisage that the two cyclisations occurring in the same direction would give either the difurano or dipyrano derivatives, respectively, while the cyclisations in opposite directions lead to the furano-pyrano product. Through the stepwise mechanism an initial indiscriminate ring closure could occur followed by the second ring closure which may also be indiscriminate, or possibly favour pyrano or furano formation depending on the identity of the ring formed by the initial ring closure. It would seem that the formation of the single pyranyl and furanyl rings are initially isokinetic (i.e., the CuO-based cycloetherification of reference 2-(naphthalen-1-yl)phenol gave the corresponding furanyl and pyranyl derivatives in 1:1 ratio, see molecules S3 and S4 in the SI) which explains why all three isomers are formed and can be isolated.

Considering the observed isomeric ratio of 58:33:9 (^{1,4}pyr₂:^{1,4}furpyr:^{1,4}fur₂) and 48:28:24 (^{1,5}pyr₂:^{1,5}furpyr:^{1,5}fur₂) it would seem that the picture is more complicated, and at some point the reaction favours the formation of dipyrano products.

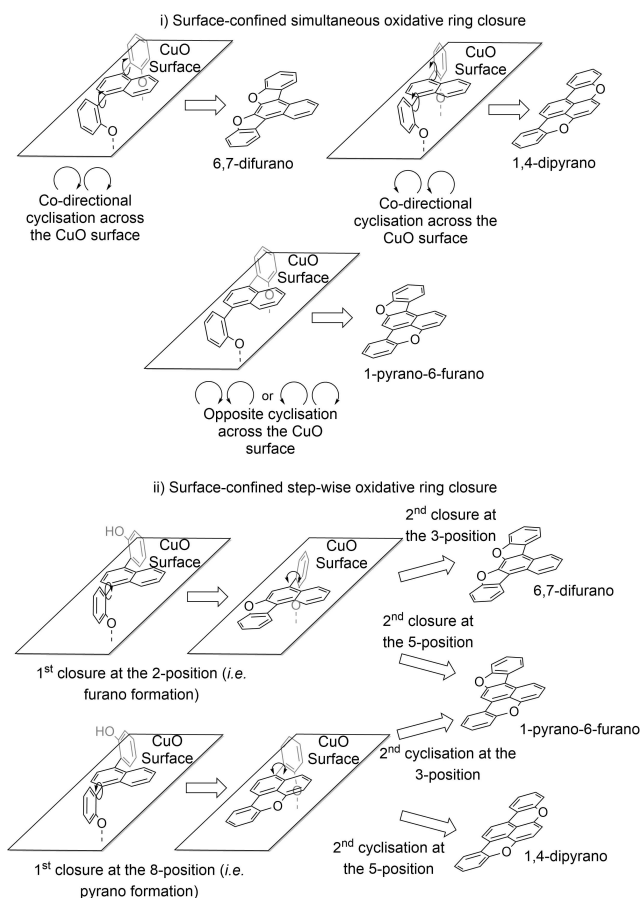


Figure 4. Schematic demonstrations depicting the possible mechanisms for the heterogenous ring closure of the 1,4-substituted naphthalenyl precursor to ${}^{1,4}\text{pyr}_2$, ${}^{1,4}\text{furpyr}$, and ${}^{1,4}\text{fur}_2$ onto a CuO surface: *i*) the simultaneous and *ii*) the stepwise ring-closure mechanisms.

It should be noted that while for 1,4-disubstituted derivatives no dealkylation side reactions were observed, a considerable amount of dealkylated (loss of a *tert*-butyl group from the naphthalene core) product was separated (around 22%) for the 1,5-substrate, thus complicating the picture further.

Optoelectronic Characterisation

Upon the isolation of the O-doped isomers, characterisation was performed fully, with particular emphasis on the photo-physical and electrochemical properties. The UV-Vis absorption and emission analyses (Figure 5, see also the excitation spectra) demonstrated that the two difuranyl molecules ${}^{1,4}\text{fur}_2$ and ${}^{1,5}\text{fur}_2$ possessed the highest-energy electronic transitions, with the lowest absorption bands (λ_{max}) centred at 361 and 364 nm, respectively (Figure 5). The double replacement of the furanyl moieties with pyranil rings caused a noticeable red shift in the UV-Vis absorption ($\lambda_{\text{max}}=467$ and 435 nm) and emission spectral envelopes ($\lambda_{\text{max}}=495$ and 443 nm) of both O-doped compounds ${}^{1,4}\text{pyr}_2$ and ${}^{1,5}\text{pyr}_2$ (Figure 5). Interestingly, hybrid derivative ${}^{1,4}\text{furpyr}$, bearing both pyranil and furanyl rings,

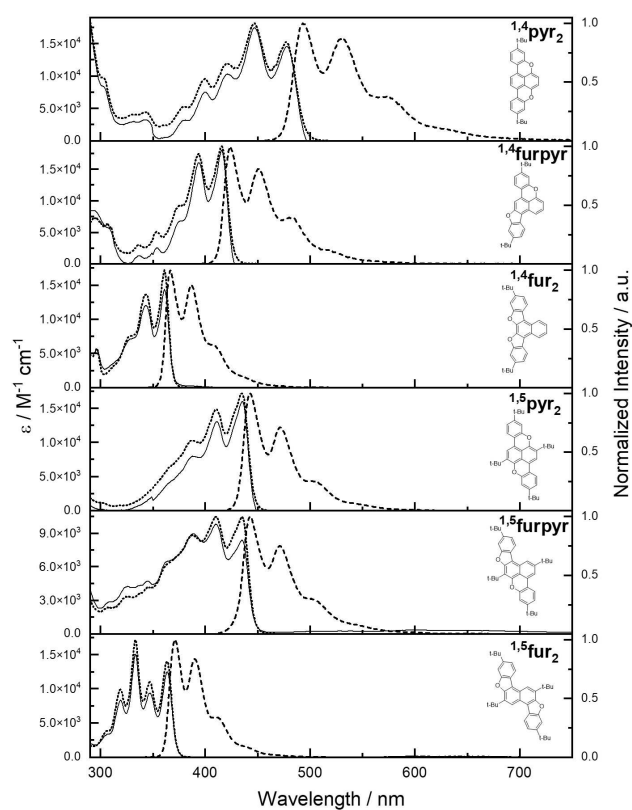


Figure 5. Molar attenuation coefficient (solid line) and normalized excitation (dotted line) and emission (dashed line) spectra of ${}^{1,4}\text{i}$ series and ${}^{1,5}\text{i}$ series. Spectra recorded in air-equilibrated benzene at r.t.

displays “intermediate” absorption and emission profiles with spectral characteristics ($\lambda_{\text{max}}=413$ nm) sitting between those of dipyrano ${}^{1,4}\text{pyr}_2$ and difurano analogue ${}^{1,4}\text{fur}_2$. Surprisingly, the spectral envelop for 1,5-furano-pyrano molecule ${}^{1,5}\text{furpyr}$ features electronic transitions from both the fingerprinting of furanyl and pyranil moieties ($\lambda_{\text{max}}=364$ and 435 nm). All derivatives showed good to very good emission quantum yields ($\Phi=77\%$, 85% , 85% for ${}^{1,4}\text{pyr}_2$, ${}^{1,4}\text{furpyr}$, ${}^{1,4}\text{fur}_2$ derivatives, respectively; $\Phi=48\%$, 57% , and 80% for ${}^{1,5}\text{pyr}_2$, ${}^{1,5}\text{furpyr}$, ${}^{1,5}\text{fur}_2$, respectively) with fluorescence lifetime values (τ) typical of PAHs ($\tau=2-6$ ns).

The results of cyclic voltammetric measurements in CH_2Cl_2 (0.1 M *n*-Bu₄NPF₆, vs. the ferrocene/ferrocenium couple Fc/Fc⁺) for all compounds are summarized in Table 1. Two reversible redox couples as oxidative events were observed for molecules ${}^{1,4}\text{pyr}_2$ and ${}^{1,5}\text{pyr}_2$ at 0.18 and 0.73 V and 0.04 and 0.62 V, respectively. One can notice that the 1,5-substitution pattern affords O-doped PAHs depicting lower oxidation potentials for the mono and double oxidation when compared to those of 1,4-derivatives ($\Delta E=0.15$ and 0.34 V for the first and second oxidation respectively; $\Delta E=E({}^{1,4}\text{pyr}_2)^{\text{ox},i}-E({}^{1,5}\text{fur}_2)^{\text{ox},j}$ where *i* is either the first or second oxidation event). When compared to the parent unsubstituted dipyrano derivative PXX,^[86] a dramatic cathodic shift of 0.59 V is observed for the first oxidation. Moreover, these O-doped naphthalene-cored derivatives clearly showed the formation of stable dicationic species, whereas PXX

Table 1. Photophysical (solvent: C₆H₆), quantum chemical, and electrochemical (solvent: CH₂Cl₂, electrolyte: 0.1 M *n*-Bu₄NPF₆, reference: Fc/Fc⁺) data for O-doped naphthalene-cored derivatives ^{1,4}i series and ^{1,5}i series.

Molecule	λ_{obs} [nm]	λ_{em} [nm]	Φ [%]	τ [ns]	S_1 calc. [nm] ^[b]	E_{HOMO} (a.u.) ^[b]	E_{LUMO} (a.u.) ^[b]	$\Delta E^{(LUMO-HOMO)}$ [b]	E_g [eV] ^[b]	E_{ox}^1 [V] ^[a]	E_{ox}^2 [V] ^[a]
^{1,4} pyr ₂	467	495	77	5.9	482	-0.187	-0.074	0.113	2.51	0.18	0.73
^{1,4} furpyr	413	426	85	3.2	407	-0.202	-0.075	0.127	2.91	0.56	n.d.
^{1,4} fur ₂	361	367	85	2.1	356	-0.216	-0.073	0.143	3.35	0.85	n.d.
^{1,5} pyr ₂	435	443	48	3.3	420	-0.188	-0.065	0.123	2.77	0.04	0.62
^{1,5} furpyr	435	442	57	3.4	397	-0.202	-0.065	0.137	2.77	0.03	0.39
^{1,5} fur ₂	364	371	80	2.2	364	-0.217	-0.075	0.142	3.32	0.83	n.d.

[a] Quoted vs. reference Fc/Fc⁺; [b] Calculated at B3LYP/6-311 + G(d,p) in CH₂Cl₂ (taken into account using PCM); n.d. = not detected.

does not show any second redox event in the potential window of CH₂Cl₂. The voltammogram of the difurano derivatives, ^{1,4}fur₂ and ^{1,5}fur₂, depicted single quasi-reversible oxidative events centred at 0.85 V and 0.83 V, respectively. For these difurano derivatives, it is apparent that the 1,4-derivative affords the lower oxidation potential ($\Delta E = 0.27$ V; $\Delta E = E^{(1,5\text{pyr}_2)^{ox}} - E^{(1,4\text{fur}_2)^{ox}}$). For the furano-pyrano molecule ^{1,5}furpyr, a similar electrochemical behaviour as that of the pyrano-pyrano derivatives was observed, with two reversible oxidation processes centred at 0.03 V and 0.38 V. Considering the electrochemical behaviour observed for ^{1,4}pyr₂ and ^{1,5}pyr₂, we hypothesized that the first and second oxidation events occurred at the pyranil moiety, whereas no furanyl-centred oxidative events are seen in the given potential window. Surprisingly, ^{1,4}furpyr displayed a quasi-reversible oxidation event at 0.56 V and no second oxidation processes could be detected. No reductive events were detected for any of the O-doped molecules in the potential window of CH₂Cl₂.

Theoretical Investigations

To shed further light on the origin of the shift of the lowest energy transition, quantum chemical density functional theory (DFT) and its time-dependent (TD-DFT) version have been used. We employed the B3LYP^[90,91] functional together with a 6-311 + G(d,p)^[92] basis set and the implicit polarizable solvent model (PCM),^[93] with CH₂Cl₂ as a solvent, to estimate the energy of the S₁ transition (further computational details in the SI).

The associated HOMO and LUMO orbital energies of the electronic ground state have been inspected to rationalize the results (Figure 7). The calculated lowest energy transitions for ^{1,4}pyr₂, ^{1,4}furpyr and ^{1,4}fur₂ are 482 nm, 407 nm and 356 nm and for ^{1,5}pyr₂, ^{1,5}furpyr and ^{1,5}fur₂ 420 nm, 397 nm and 364 nm, respectively. The HOMO and LUMO orbital energies and shapes indicate a destabilization of the HOMO in the series ^{1,4}fur₂ to ^{1,4}pyr₂ and from ^{1,5}fur₂ to ^{1,5}pyr₂, (see Table S1 and Figure 6) due to the formation of a six-membered, O-containing, antiaromatic ring, which nicely correlates with the decrease of the excitation wavelength.

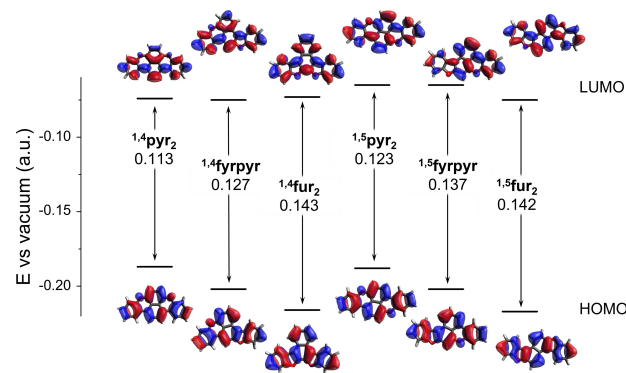


Figure 6. Calculated HOMO and LUMO of ^{1,4}i series and ^{1,5}i series synthesised O-doped PAHs along with their associated energy gap in eV.

Electrochromic Studies

Following on from the CV analysis, spectroelectrochemical analyses were performed to investigate the chromogenic properties of the most representative derivatives. Molecules ^{1,4}pyr₂, ^{1,4}furpyr, and ^{1,5}fur₂ were chosen to be taken forward for this study (Figure 7 and Figure 8, for full spectra see SI). The spectroelectrochemical analysis of ^{1,4}pyr₂ demonstrated that, upon oxidation at 0.9 V (vs. Ag/AgCl) to the radical cation state, a dramatic red-shift of 230 nm of the absorption maxima was seen along with a decrease of intensity of the peak at

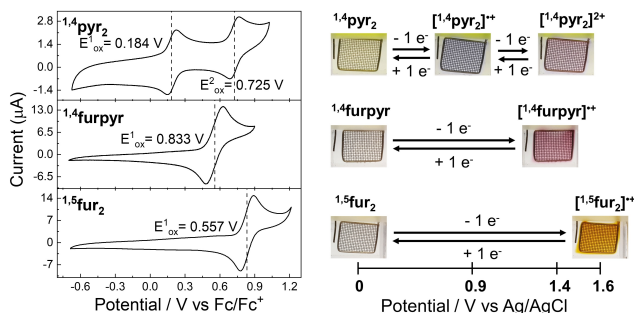


Figure 7. Cyclic voltammograms (0.1 M *n*-Bu₄NPF₆ in CH₂Cl₂) of ^{1,4}pyr₂, ^{1,4}furpyr, and ^{1,5}fur₂ (left) and pictures of the colour change observed at the platinum grid working electrode during the spectroelectrochemical analysis (right).

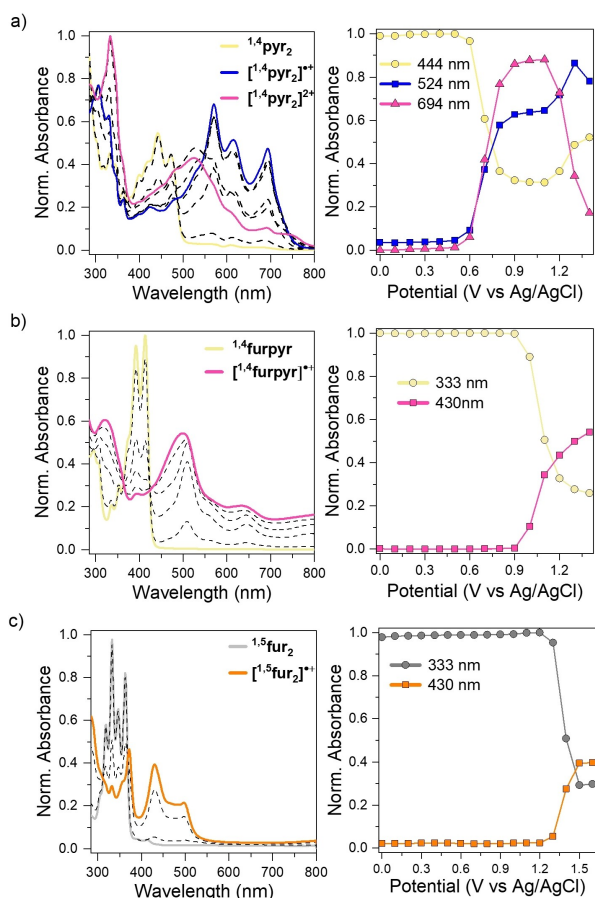


Figure 8. Spectroelectrochemical investigations of compounds a) $1,4\text{-pyr}_2$ ($c = 0.007$ mM), b) $1,4\text{-furpyr}$ ($c = 0.14$ mM), and c) $1,5\text{-fur}_2$ ($c = 0.17$ mM) in CH_2Cl_2 . Experimental conditions: platinum minigrad working electrode, platinum wire auxiliary electrode, Ag/AgCl reference electrode and 0.1 M $n\text{-Bu}_4\text{NPF}_6$ as supporting electrolyte.

approximately 450 nm belonging to the neutral state (Figure 8a).

With this shift of absorption maxima came a change in the colour of the solution from bright yellow to deep blue that returns to pale yellow slowly upon removing the applied potential (Figure 7). Further oxidation at 1.4 V (vs. Ag/AgCl) to the dication state gave rise to an almost pink colour (Figure 7), which was associated with a loss of intensity of the electronic transition in the range between 550 and 750 nm and the rise of a broad absorption peak centred at around 525 nm (Figure 8a). A similar pink colour was achieved while performing the spectroelectrochemical analysis of $1,4\text{-furpyr}$ (Figure 7), however this was due to the formation of the radical cation state. Upon application of a potential value of 1.4 V (vs. Ag/AgCl) to a pale-yellow solution of $1,4\text{-furpyr}$, the characteristic absorption envelop from 350 to 425 nm lessened and a new electronic transition centred at 500 nm appeared (Figure 8b).

Upon performing the spectroelectrochemical analysis of the difurano molecule $1,5\text{-fur}_2$ (Figure 8c), it was found that a colourless to orange colour could be observed (Figure 7). When $1,5\text{-fur}_2$ was subjected to a potential of 1.6 V (vs. Ag/AgCl), a loss

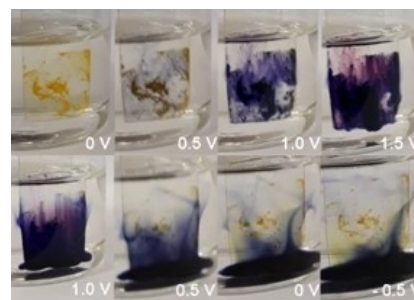


Figure 9. Pictures taken of spectroelectrochemical analysis experiment using $1,4\text{-pyr}_2$ in a thin film demonstrating loss of adhesion of the deposited layer upon application of potential. Thin films created by drop-casting a solution of $1,4\text{-pyr}_2$ in CH_2Cl_2 onto PET/ITO, Ag/Ag⁺ used as the reference and Pt as a counter electrode. The substrate was suspended in 0.1 M LiClO_4 in MeCN.

of intensity of the spectral region between 300 and 375 nm was seen along with a progressive growth of a transition at approximately 425 nm depicting a shoulder at 500 nm (Figure 8c).

The spectroelectrochemical analysis of $1,4\text{-pyr}_2$ was also performed with the material deposited as a thin film on a PET/ITO working electrode. The thin film was submerged in a 0.1 M LiClO_4 solution and the spectroelectrochemical experiment repeated. This led to a colour change of the thin film from yellow to deep blue, however this oxidation caused the film to become soluble in the electrolyte and 'shed' from the electrode (Figure 9). As the loss of adhesion of the electrochrome to the PET/ITO electrode would lead to dramatic shortening of the lifetime of an ECD, we are now developing alternative strategies to anchor the electrochrome on a stable framework to avoid such colour bleaching. Overall, the results of these spectroelectrochemical analyses show that these O-doped materials can hold great promises for engineering coloured electrochromic devices due to their large shift in the absorption spectra and very low operative oxidation potentials.

Conclusion

In conclusion, through this work we were able to synthesise and isolate six different O-doped small molecules. Our synthetic work demonstrated that, through use of CuO-mediated intramolecular etherification reaction of 1,4- or 1,5-disubstituted naphthalenyl-cored precursors, not only could the desired pyrano moieties be obtained but so could furano containing molecules. Subsequently, this led to the isolation of six O-doped PAHs, among which two possessed both pyrano and furano moieties. Interestingly, the furano-pyrano hybrid derivatives depicted intermediate absorption maxima when compared to the difurano and dipyrano analogues, as well as intermediate electrochemical properties. In both derivative series, the dipyrano O-doped PAHs showed strong bathochromically-shifted absorption envelopes, with the difuranyl products being highest energy absorption structures. Computational investigations showed that the pyrano annulation has the strongest

effect on the destabilisation of the HOMO energy level, that is reflected in a shrinking of the HOMO-LUMO gap. All synthesised O-doped PAHs were shown to be electroactive, featuring *p*-type semiconducting properties with low oxidation potentials. Spectroelectrochemical analysis of selected derivatives, ^{1,4}pyr₂, ^{1,4}furpyr, and ^{1,5}fur₂, showed that the molecules undergo a dramatic red shift of the absorption maxima upon oxidation to their respective radical cation states, and return to the original absorption spectrum. Depending on the type of O-ring (i.e., pyrano or furano), different electrochromic transitions at different potentials could be observed, with the furanyl-containing structures featuring transparent-to-colour changes (to pink or orange depending on the structure). Given the low oxidation potentials and high electrochromic contrast, these O-doped small molecules represent valuable candidates for engineering electrochromic displays. It is with this objectives in mind that we are currently attempting to integrate these molecules in electrochromic devices and study their performances.

Experimental Section

General Remarks

Thin layer chromatography (TLC) was performed using pre-coated aluminium sheets using 0.20 mm silica gel 60 with fluorescent indicator F254 manufactured by Merck. Column chromatography was carried out using silica gel 60 (particle size 40–60 μm) from Applichem or using neutral Al₂O₃ supplied by Carlo Erba Reagents. Melting Points (mp) were measured, uncorrected, on a Stuart SMP1 analogue melting point apparatus. Nuclear Magnetic Resonance (NMR) spectra were recorded using a Bruker Fourier 300 MHz spectrometer equipped with a dual (¹³C, ¹H) probe, a Bruker Fourier 400 MHz equipped with a broadband multinuclear (BBO) probe, a Bruker AV III HDX 700 NMR spectrometer (Bruker BioSpin, Rheinstetten, Germany). ¹H spectra were obtained at 700 MHz, 600 MHz, 400 MHz or 300 MHz and ¹³C at 176 MHz, 151 MHz 126 MHz, 101 MHz or 75 MHz with complete decoupling for proton. All spectra were obtained at room temperature unless otherwise specified. Chemical shifts were reported in ppm according to tetramethylsilane using the solvent residual signal as an internal reference (CDCl₃: δ_H = 7.26 ppm, C₆D₆: δ_H = 7.16 ppm, δ_C = 128.06 ppm; CD₂Cl₂: δ_H = 5.32 ppm, δ_C = 53.5 ppm). The splitting of peaks is described as s (singlet), d (doublet), t (triplet), dd (doublet of doublets), and m (multiplet). Infrared spectra (IR) (IR) were recorded on a Shimadzu IR Affinity 15 FTIR spectrometer in ATR mode with a diamond monocrystal at Cardiff University. Mass Spectrometry (MS): High resolution ESI mass spectra (HRMS) were performed on a Waters LCT HR TOF mass spectrometer in the positive or negative ion mode at Cardiff University or at the University of Vienna on a maXis UHR ESI-Qq-TOF mass spectrometer (Bruker Daltonics, Bremen, Germany) in the positive or negative ion mode by direct infusion. The sum formulas of the detected ions were determined using Bruker Compass DataAnalysis 4.1 based on the mass accuracy (Δ*m/z* ≤ 5 ppm) and isotopic pattern matching (SmartFormula algorithm). HRLDMS spectra were acquired on a timsTOF fleX ESI/MALDI dual source-trapped ion mobility separation – Qq-TOF mass spectrometer (Bruker Daltonics, Bremen, Germany) in the positive ion mode. The sum formulas of the detected ions were determined using Bruker Compass DataAnalysis 5.3 based on the mass accuracy (Δ*m/z* ≤ 5 ppm) and isotopic pattern matching (SmartFormula algorithm). UV-Vis Absorption spectroscopy: was recorded on Agilent Cary 5000 UV-Vis-NIR Spectrophotometer running in double beam mode with a

matched pair of quartz absorbance cuvettes (1 × 1 cm). All absorption measurements were performed at 21 °C unless specified otherwise. Steady-state photoluminescence: photoluminescence (PL) excitation and emission spectra, absolute quantum yield, and decay curves were recorded on a FLS1000 photoluminescence spectrometer from Edinburgh Instruments. The spectrometer was equipped with excitation and emission double grating Czerny-Turner monochromators, a continuous 400 W xenon lamp, and a photomultiplier detector with extended near-infrared sensitivity (PMT-980), thermoelectric cooled to –20 °C with a Peltier element. For fluorescence decay measurement the spectrometer was fitted with a picosecond pulsed light emitting diode (ELED-295) or with a picosecond pulsed diode laser (EPL-405). Cyclic voltammetry: experiments were performed at room temperature in dry argon-purged CH₂Cl₂ (dried over activated molecular sieves prior to use) using an Autolab PGSTAT204 potentiostat. Dry argon was bubbled through the sample solution for at least 15 min prior to each measurement and the headspace was continuously flushed throughout the experiment. A pre-bubbler filled with CH₂Cl₂ was used in order to prevent solvent evaporation. Glassy carbon (3 mm diameter) was used as a working electrode, Pt wire as auxiliary electrode, and an Ag/AgCl electrode was used as reference. The glassy carbon electrode was sequentially polished on a pad using 15, 3 and 1 μm diamond slurry and washed with deionized water and methanol before each experiment; the Pt wire was flame-cleaned. Tetrabutylammonium hexafluorophosphate was recrystallized twice from absolute ethanol prior to use and it was added to the solution as a supporting electrolyte at a concentration of 0.1 M. Ferrocene (sublimed at reduced pressure) is used as an internal reference (E_{Fc/Fc+} = 0.00 V). Spectroelectrochemical characterisation was performed using a thin layer quartz cuvette (path length of 0.5 mm) equipped with an optically transparent platinum minigrid working electrode, platinum wire auxiliary electrode, and an Ag/AgCl reference electrode.

Degassing of solutions/solvent mixtures was done by bubbling nitrogen through the solution with sonication followed by sealing the system under an inert atmosphere. Anhydrous conditions were achieved through heating of round bottom flasks to 100 °C in the oven overnight, and allowing to cool under vacuum, followed by purging with nitrogen. Anhydrous solvents were dried over activated molecular sieves for at least 24 hours prior to use. Low temperatures were achieved using low temperature baths: –84 °C with ethyl acetate/liquid nitrogen, –35 °C with Et₂O/liquid nitrogen while monitoring the temperature with a low temperature thermometer, 0 °C with ice/H₂O. Inert atmosphere was maintained using nitrogen-filled balloons equipped with a syringe and needle which was used to pierce the silicone stoppers used to seal the flask's necks. Chemicals were purchased from Sigma Aldrich, TCI, Alfa Aesar, or Flurochem and used as supplied except naphthoquinone which was purified by recrystallization from hexane prior to use. Basified SiO₂ for column chromatography was produced by suspending the silica in the desired eluent and 2% NEt₃ then adding it to the column, followed by flushing a volume of the eluent with 2% NEt₃ equal to the volume of silica used.

Synthesis

1-Bromo-4-(*tert*-butyl)-2-methoxybenzene (1):^[94] 2-bromo-5-(*tert*-butyl)phenol (1.45 g, 6.3 mmol) along with oven-dried K₂CO₃ (2.72 g, 19.7 mmol) were weighed into a round bottom flask. The flask was flushed with nitrogen and dry DMF (8 ml) was added, followed by Mel (1.87 g, 13.2 mmol). The flask was heated to 55 °C for 42 h, after which the reaction was cooled to r.t. and any excess Mel was quenched with 1 M aq. NaOH. The mixture was diluted with water and the crude extracted with EtOAc (3 × 40 ml). After this the organic layers were combined and washed with 1 M NaOH,

water, and brine; the product was dried over MgSO_4 and concentrated in vacuo. This yielded 1.20 g (4.9 mmol, 78%) of pale-yellow crystalline material which required no further purification. M.p.: 38–40 °C; ^1H NMR (400 MHz, CDCl_3) δ 7.44 (d, $J=8.3$ Hz, 1H), 6.93 (d, $J=1.8$ Hz, 1H), 6.87 (dd, $J=8.3, 1.9$ Hz, 1H), 3.91 (s, 3H), 1.32 (s, 9H); ^{13}C NMR (101 MHz, CDCl_3) δ 155.5, 152.3, 132.6, 119.1, 109.7, 108.5, 56.1, 34.9, 31.3; MS (EI m/z): found 242.03, required 242.03; characterisation in accordance with literature.^[94]

(4-(*tert*-Butyl)-2-methoxyphenyl)boronic acid (2):^[81] 1-bromo-4-(*tert*-butyl)-2-methoxybenzene (510 mg, 2.1 mmol) was weighed into an oven-dried round bottom flask which was put under a nitrogen atmosphere. Dry THF (5 ml) was added and the system was cooled to -78°C , after which *n*-BuLi (1.4 ml, 2.2 mmol) was added. $\text{B}(\text{OMe})_3$ (370 mg, 3.6 mmol) was added and the reaction mixture was warmed to r.t. for 23 h. The reaction was quenched with 1 M HCl then diluted with water and the organic components extracted using EtOAc (3×30 ml). The organic layers were combined, dried over MgSO_4 , and concentrated in vacuo. Purification by column chromatography (SiO_2 ; eluent: Hexane/Et₂O 8:2) yielded 360 mg (1.75 mmol, 84%) of the desired product as a white solid. M.p.: 105–108 °C; ^1H NMR (400 MHz, CDCl_3) δ 7.78 (d, $J=7.7$ Hz, 1H), 7.09 (dd, $J=7.7, 1.4$ Hz, 1H), 6.95 (d, 1H), 5.68 (s, 2H), 3.96 (s, 3H), 1.36 (s, 9H); ^{13}C NMR (101 MHz, CDCl_3) δ 164.6, 156.8, 136.5, 118.4, 107.2, 55.4, 35.2, 31.2, carbon bound to the boron is not seen; HRMS (ES m/z): $[\text{M}+\text{H}]^+$ calc. for $\text{C}_{11}\text{H}_{18}\text{BO}_3$: 209.1349, found 209.1352; FTIR (ATR) ν (cm^{-1}): 3535, 3419, 3213, 3010, 2953, 2841, 1610, 1556, 1506, 1471, 1450, 1408, 1363, 1325, 1280, 1263, 1217, 1199, 1178, 1159, 1120, 1049, 997, 904, 850, 821, 750, 717, 667, 653, 634, 615, 567, 538.^[81]

1,4-Dibromonaphthalene (5):^[88] Naphthalene (210 mg, 1.6 mmol) was weighed into a round bottom flask, dry CH_2Cl_2 was added and the flask was cooled to -35°C in the dark. Br_2 (740 mg, 4.7 mmol) was added slowly and the reaction was left in the cooling bath overnight. The temperature had risen to 10°C overnight so the reaction was quenched by addition of sat. aq. $\text{Na}_2\text{S}_2\text{O}_3$. It was further diluted with water and the crude extracted with CH_2Cl_2 (3×30 ml). The organic layers were combined and washed with water, sat. aq. $\text{Na}_2\text{S}_2\text{O}_3$, and 0.1 M aq. NaOH. The crude was dried over MgSO_4 , concentrated in vacuo, and purified by column chromatography (SiO_2 ; eluent: Hexane). This yielded 280 mg (0.98 mmol, 61%) of the desired product as white crystals. M.p.: 77–79 °C; ^1H NMR (400 MHz, CDCl_3) δ 8.29 (dd, $J=6.4, 3.3$ Hz, 2H), 7.74–7.63 (m, 2H), 7.28 (s, 2H); ^{13}C NMR (101 MHz, CDCl_3) δ 133.0, 130.1, 128.2, 127.8, 122.6; MS (EI, m/z) found: 285.88, required: 285.88; characterisation in accordance with literature.^[88]

1,4-Bis(4-(*tert*-butyl)-2-methoxyphenyl)naphthalene (6): 1,4-dibromonaphthalene (63 mg, 0.2 mmol), **2** (136 mg, 0.7 mmol), and K_2CO_3 (122 mg, 0.9 mmol) were weighed into a round bottom flask which was flushed with nitrogen. A degassed mixture of dioxane and water (4:1) was added followed by $[\text{Pd}(\text{PPh}_3)_4]$ (13 mg, 0.01 mmol) under a flow of nitrogen. The reaction mixture was heated to 85°C for 6.5 h. The reaction mixture was cooled to r.t. then diluted with water and the crude was extracted with CH_2Cl_2 (3×25 ml). The crude was dried over MgSO_4 , concentrated in vacuo, and purified by column chromatography (SiO_2 ; eluent: Hexane/ CH_2Cl_2 9:1 to Hexane/ CH_2Cl_2 8:2). This yielded 93 mg (0.2 mmol, 93%) of the desired product as a white crystalline material. M.p.: 201–204 °C; ^1H NMR (400 MHz, CDCl_3) δ 7.70–7.60 (m, 2H), 7.44 (d, $J=1.9$ Hz, 2H), 7.38–7.31 (m, 2H), 7.29 (d, $J=7.8$ Hz, 1H), 7.25 (d, $J=9.0$ Hz, 2H, integral inaccurate due to overlap with solvent peak), 7.15–7.05 (m, 4H), 3.74 (d, $J=1.9$ Hz, 6H), 1.43 (s, 18H); ^{13}C NMR (101 MHz, CDCl_3) δ 157.0, 157.0, 152.3, 136.4, 136.3, 132.3, 131.7, 127.0, 127.0, 126.9, 126.8, 125.1, 117.6, 117.5, 108.6, 108.5, 55.7, 55.6, 35.0, 31.5; HRMS (ES m/z): $[\text{M}+\text{H}]^+$ calc. for $\text{C}_{32}\text{H}_{37}\text{O}_2$: 453.2794, found: 453.2797; FTIR (ATR) ν (cm^{-1}): 2951, 2927, 2899,

2862, 2831, 2362, 1608, 1558, 1498, 1456, 1402, 1381, 1361, 1280, 1261, 1228, 1145, 1116, 1091, 1035, 974, 904, 852, 842, 817, 767, 655.

6,6'-(Naphthalene-1,4-diyl)bis(3-(*tert*-butyl)phenol) (7): **6** (119 mg, 0.2 mmol) was weighed into a flask then put under a nitrogen atmosphere. Dry CH_2Cl_2 was added and the system was stirred until all solids had dissolved. The flask was covered with aluminium foil and cooled to -78°C . BBr_3 (1.3 ml, 1.3 mmol) was added slowly and the reaction was then allowed to stir at r.t. overnight. The reaction was quenched with careful addition of sat. aq. NaHCO_3 solution and diluted further with water. The crude was extracted using CH_2Cl_2 (3×20 ml), dried over MgSO_4 , and concentrated in vacuo. Purification by column chromatography (SiO_2 ; eluent: CH_2Cl_2) yielded 87 mg (0.2 mmol, 78%) of an isomeric mixture of the desired product as a white solid. M.p.: 124–126 °C; ^1H NMR (400 MHz, CDCl_3) δ 7.87–7.78 (m, 2H), 7.60 (d, $J=1.5$ Hz, 2H), 7.55–7.49 (m, 2H), 7.30–7.23 (m, 2H), 7.18–7.10 (m, 2H), 4.89 (s, 1H), 4.84 (s, 1H), 1.44 (s, 18H); ^{13}C NMR (101 MHz, CDCl_3) δ 153.4, 152.8, 152.7, 135.0, 134.9, 132.5, 132.5, 130.9, 130.7, 128.2, 127.0, 127.0, 126.5, 126.4, 123.1, 117.9, 117.8, 112.9, 112.9, 34.8, 31.4; HRMS (ES m/z): $[\text{M}+\text{H}]^+$ calc. for $\text{C}_{30}\text{H}_{33}\text{O}_2$: 424.2481, found: 424.2477; FTIR (ATR) ν (cm^{-1}): 3566, 3425, 3215, 2954, 2902, 2866, 1614, 1558, 1508, 1500, 1481, 1456, 1404, 1386, 1361, 1311, 1263, 1211, 1141, 1130, 1114, 1080, 1026, 977, 939, 923, 794, 765, 744, 702, 648.

Synthesis of $^{1,4}\text{pyr}_2$, $^{1,4}\text{furpyr}$, and $^{1,4}\text{fur}_2$: **7** (137 mg, 0.32 mmol) was weighed into a round bottom flask, along with CuO (255 mg, 3.21 mmol). PhNO_2 (3 ml) was added, and the reaction mixture was heated to 220°C overnight under air. The solvent was distilled off, the crude was dissolved in CH_2Cl_2 and filtered over celite. The crude then underwent column chromatography (Basified SiO_2 ; eluent: Hex) to purify the three possible isomers together before further separation by HPLC. The overall yield of the 3 isomers was 89 mg (0.21 mmol, 66%)

3,10-Di-*tert*-butylbenzo[3,4]isochromeno[7,8,1-*mn*]xanthene ($^{1,4}\text{pyr}_2$): product obtained as an orange solid after purification by HPLC (8.6 mg injected) 4.9 mg obtained (0.012 mmol, 4%). Orange crystals were obtained by recrystallization from $\text{CH}_2\text{Cl}_2/\text{MeOH}$. M.p.: $> 250^\circ\text{C}$; ^1H NMR (700 MHz, CD_2Cl_2) δ 7.56 (d, $J=8.3$ Hz, 2H), 7.34 (s, 2H), 7.07 (dd, $J=8.2, 1.6$ Hz, 2H), 6.94 (d, $J=1.9$ Hz, 2H), 6.66 (s, 2H), 1.32 (s, 18H); ^{13}C NMR (101 MHz, CDCl_3) δ 152.8, 151.6, 144.3, 124.6, 121.8, 120.9, 119.6, 116.8, 114.3, 112.9, 107.6, 33.7, 30.0; HRMS (ES, m/z): $[\text{M}]^+$ calc. for $\text{C}_{30}\text{H}_{28}\text{O}_2$: 420.2089, found: 420.2086; FTIR (ATR) ν (cm^{-1}): 2953, 2922, 2852, 2360, 2331, 1843, 1734, 1716, 1683, 1668, 1653, 1635, 1591, 1570, 1506, 1463, 1423, 1369, 1303, 1274, 1255, 1234, 1201, 1159, 1138, 1093, 1041, 1020, 948, 921, 875, 864, 821, 806, 783, 702, 671, 632, 584, 555, 536; UV/Vis (C_6H_6): λ_{max} (ϵ) = 473 (12400), 444 (15000), 419 (9900), 399 (7700), 380 (4200), 342 (3500), 285 (20300), 262 nm ($16700 \text{ dm}^3 \text{ mol}^{-1} \text{ cm}^{-1}$).

6,12-Di-*tert*-butylbenzo[2,3]benzofuro[4,5,6-*kl*]xanthene ($^{1,4}\text{furpyr}$): product was obtained as a yellow solid after purification by HPLC (8.6 mg injected), 2.8 mg obtained (0.007 mmol, 22% representative). ^1H NMR (700 MHz, CD_2Cl_2) δ 8.18 (d, $J=8.2$ Hz, 1H), 8.10–8.01 (m, 1H), 7.95–7.82 (m, 2H), 7.71 (d, $J=1.5$ Hz, 1H), 7.63 (t, $J=7.9$ Hz, 1H), 7.55 (dd, $J=8.2, 1.7$ Hz, 1H), 7.27 (dd, $J=8.3, 1.9$ Hz, 1H), 7.21 (d, $J=1.9$ Hz, 1H), 7.04 (dd, $J=7.7, 0.8$ Hz, 1H), 1.45 (s, 9H), 1.38 (s, 9H); ^{13}C NMR (126 MHz, CDCl_3) δ 156.3, 156.0, 154.1, 152.2, 151.6, 149.8, 130.6, 128.9, 127.6, 122.6, 122.2, 121.1, 121.0, 120.7, 117.9, 116.0, 114.1, 108.4, 107.56, 100.45, 35.22, 34.89, 31.7, 31.1; HRMS (CI, m/z): $[\text{M}]^+$ calc. for $\text{C}_{30}\text{H}_{28}\text{O}_2$: 420.2084, found: 420.2087; FTIR (ATR) ν (cm^{-1}): 2953, 2922, 2852, 2360, 2331, 1843, 1734, 1716, 1683, 1668, 1653, 1635, 1591, 1570, 1506, 1463, 1423, 1369, 1303, 1274, 1255, 1234, 1201, 1159, 1138, 1093, 1041, 1020, 948, 921, 875, 864, 821, 806, 783, 702, 671, 632, 584, 555, 536; UV/Vis (C_6H_6): λ_{max}

(ϵ)=413 (17500), 392 (16400), 353 (4900), 337 (7700), 307 (6300), 294 (7700), 268 nm (15900 dm³mol⁻¹cm⁻¹).

2,11-Di-*tert*-butylnaphtho[2,1-b:3,4-b']bisbenzofuran (^{1,4}fur₂): The title molecule was obtained as a white solid after purification by HPLC (12.0 mg injected), 0.8 mg obtained (0.002 mmol, <1%). ¹H NMR (700 MHz, CD₂Cl₂) δ 8.84–8.78 (m, 2H), 8.40 (d, J =8.2 Hz, 2H), 7.87 (d, J =1.5 Hz, 2H), 7.82–7.76 (m, 2H), 7.63 (dd, J =8.2, 1.7 Hz, 2H), 1.48 (s, 18H); ¹³C DEPT NMR (176 MHz, CD₂Cl₂) δ 156.8, 150.6, 141.3, 126.3, 125.4, 124.6, 122.3, 121.6, 121.1, 118.4, 109.0, 35.2, 31.4; HRMS (MALDI, m/z): [M]⁺ calc. for C₃₀H₂₈O₂ 420.2084, found: 420.2081; FTIR (ATR) ν (cm⁻¹): 2953, 2923, 2852, 2361, 2332, 1844, 1734, 1717, 1684, 1668, 1653, 1636, 1591, 1570, 1506, 1464, 1423, 1369, 1304, 1275, 1256, 1234, 1202, 1159, 1138, 1094, 1042, 1020, 949, 922, 876, 864, 822, 806, 783, 702, 671, 633, 584, 555, 536; UV/Vis (C₆H₆): λ_{\max} (ϵ)=361 (14380), 343 (12011), 328 (7100), 297 nm (9829 dm³mol⁻¹cm⁻¹).

1,5-Dibromo-3,7-di-*tert*-butylnaphthalene (**8**):^[89] 2,6-di-*tert*-butylnaphthalene (1.00 g, 4.16 mmol) and AlCl₃ (3 mg, 0.02 mmol) were dissolved in CH₂Cl₂ (6 ml) under an inert atmosphere. To this, a solution of Br₂ (0.45 ml, 8.79 mmol) in CH₂Cl₂ (6 ml) was added and the reaction was left to stir at room temperature for 24 h. After quenching with sat. aq. Na₂S₂O₃ solution, the organic layer was diluted with CH₂Cl₂ (75 ml), washed with sat. aq. Na₂S₂O₃ (2 × 100 ml), water (2 × 100 ml), and brine (1 × 100 ml). The product was then dried over Na₂SO₄ and concentrated in vacuo. This yielded 1.463 g (3.67 mmol, 88%) of the desired product as a white solid. M.p.: 202–204 °C; ¹H NMR (300 MHz, CDCl₃) δ 8.12 (m, 2H), 7.89 (m, 2H), 1.42 (s, 18H); ¹³C NMR (75 MHz, CDCl₃) δ 150.1, 131.0, 129.9, 123.1, 122.3, 35.2, 31.2; MS (EI m/z): found: 298.00, required: 298.01.^[89]

3,7-Di-*tert*-butyl-1,5-bis(4-(*tert*-butyl)-2-methoxyphenyl)naphthalene (**9**): **8** (273 mg, 0.69 mmol), **2** (485 mg, 2.32 mmol), and K₂CO₃ (438 mg, 3.17 mmol) were dissolved in a degassed mixture of dioxane and H₂O (15 ml:3 ml). [Pd(PPh₃)₄] (31 mg, 0.03 mmol) was added and the reaction heated to 85 °C for 20 h before being cooled and diluted with water. The crude product was extracted with CH₂Cl₂ (3 × 50 ml), dried over Na₂SO₄, concentrated in vacuo, and purified by column chromatography (SiO₂; eluent: Pet Et to Pet Et/CH₂Cl₂ 8:2). This yielded 281 mg (0.39 mmol, 56%) of the desired product as a white solid. M.p. 227–228 °C; ¹H NMR (300 MHz, CDCl₃) δ 7.63–7.57 (m, 2H), 7.51 (dd, J =3.2, 2.3 Hz, 2H), 7.36 (d, J =7.8 Hz, 1H), 7.32 (d, J =7.7 Hz, 1H), 7.20–7.10 (m, 4H), 3.81 (d, J =3.6 Hz, 6H), 1.49 (s, 18H), 1.35 (s, 18H); ¹³C NMR (75 MHz, CDCl₃) δ 156.9, 156.9, 152.0, 146.4, 146.4, 136.4, 131.9, 130.1, 129.9, 127.8, 126.4, 121.2, 121.0, 117.5, 117.4, 108.4, 108.2, 55.5, 35.0, 34.8, 31.6, 31.3; HRMS (ES m/z) [M+H]⁺ calc. for C₄₀H₅₃O₂, 565.4046 found: 565.4036; FTIR (ATR) ν (cm⁻¹): 2953, 2900, 2864, 1606, 1560, 1521, 1506, 1489, 1473, 1458, 1396, 1362, 1285, 1267, 1229, 1202, 1180, 1155, 1134, 1125, 1086, 1038, 1005, 951, 912, 885, 849, 824, 812, 783, 731, 704, 685, 660, 576, 549, 503, 470, 462.

6,6'-(3,7-Di-*tert*-butylnaphthalene-1,5-diyl)bis(3-(*tert*-butyl)phenol) (**10**): **9** (260 mg, 0.46 mmol) was weighed into an oven-dried round bottom flask and put under a nitrogen atmosphere. The flask was covered to minimise the exposure to light and the system cooled to –78 °C. BBr₃ (1.8 ml, 1.80 mmol) was added and the reaction warmed to room temperature for 4 h before being quenched by the dropwise addition of water. The crude was extracted with CH₂Cl₂ (3 × 30 ml), dried over Na₂SO₄, concentrated in vacuo, and purified by column chromatography (SiO₂; eluent: Pet Et/CH₂Cl₂ 7:3 to Pet Et/CH₂Cl₂ 3:7). This yielded 118 mg (0.22 mmol, 48%) of the desired product as a white solid. M.p. >250 °C; ¹H NMR (300 MHz, CDCl₃) δ 7.68 (dd, J =2.1, 1.6 Hz, 2H), 7.59 (d, J =1.8 Hz, 2H), 7.27 (m, 3H due to solvent peak overlap), 7.17–7.09 (m, 4H), 4.92 (s, 1H), 4.87 (s, 1H), 1.42 (s, 18H), 1.31 (s,

18H) NMR suggests a mixture of isomers present; ¹³C NMR (75 MHz, CDCl₃) δ 153.2, 152.8, 148.8, 134.3, 134.3, 130.8, 130.8, 130.5, 127.8, 123.8, 121.1, 117.7, 112.7, 35.0, 34.8, 31.4, 31.2; HRMS (ES m/z) [M]⁺ calc. for C₃₈H₄₈O₂, 536.3654 found: 536.3658; IR ν (cm⁻¹): 3547, 3523, 3439, 2960, 1772, 1624, 1598, 1560, 1508, 1473, 1458, 1400, 1361, 1305, 1267, 1249, 1188, 1153, 1130, 1116, 1097, 1076, 1022, 937, 920, 891, 875, 783, 705, 688, 661, 599, 549, 518, 472, 418.

Synthesis of ^{1,5}pyr₂, ^{1,5}furpyr, and ^{1,5}fur₂: **10** (88 mg, 0.16 mmol) was weighed into a round bottom flask, along with CuO (130 mg, 1.63 mmol). PhNO₂ (1.6 ml) was added, and the reaction mixture was heated to 220 °C overnight under air. The solvent was distilled off, the crude was dissolved in CH₂Cl₂ and filtered over celite. The crude then underwent column chromatography (Basified SiO₂; eluent: Hex) to purify the three possible isomers together before further separation by HPLC. 52 mg of a mixture of 5 products was obtained: ^{1,5}pyr₂, ^{1,5}furpyr, ^{1,5}fur₂, and two de-*tert*-butylated isomers.

2,6,9,13-Tetra-*tert*-butylxantheno[2,1,9-mna]xanthene (^{1,5}pyr₂): after purification by HPLC (13.6 mg injected), 4.2 mg (0.008 mmol, 5%) of the title compound was isolated as an orange solid. ¹H NMR (700 MHz, C₆D₆) δ 7.55 (d, J =8.3 Hz, 2H), 7.53 (s, 2H), 6.97 (dd, J =8.3 Hz, 1.9 Hz, 2H), final aromatic proton hidden by solvent peak, 1.50 (s, 18H), 1.33 (s, 18H); ¹³C NMR (101 MHz, C₆D₆) δ 152.2, 148.1, 129.0, 128.3, 123.2, 121.6, 120.8, 119.2, 119.1, 114.8, 113.5, 34.4, 34.1, 30.7, 29.5; HRMS (ES m/z): [M]⁺ calc. for C₃₈H₄₄O₂, 532.3336 found: 523.3320; FTIR (ATR) ν (cm⁻¹): 2954, 2902, 2866, 1728, 1627, 1618, 1570, 1517, 1462, 1425, 1392, 1361, 1307, 1261, 1236, 1226, 1207, 1166, 1120, 1083, 1062, 1026, 925, 866, 808, 763, 736, 675, 657, 601, 547, 505, 459, 414. UV/Vis (C₆H₆): λ_{\max} (ϵ)=435 (29636), 411 (24129), 388 (14722), 365 (7480), 275 nm (9000 dm³mol⁻¹cm⁻¹).

2,6,9,12-Tetra-*tert*-butylbenzo[mn]benzofuro[3,2-b]xanthene (^{1,5}furpyr): After purification by HPLC (13.6 mg injected), 2.4 mg (0.005 mmol, 3%) of the title compound was isolated as a yellow solid ¹H NMR (600 MHz, CD₂Cl₂) δ 8.24 (d, J =1.5 Hz, 1H), 8.17 (d, J =8.2 Hz, 1H), 7.93 (d, J =8.3 Hz, 1H), 7.80 (d, J =1.4 Hz, 1H), 7.68 (d, J =1.5 Hz, 1H), 7.51 (dd, J =8.2, 1.6 Hz, 1H), 7.24 (dd, J =8.3, 1.9 Hz, 1H), 7.20 (d, J =1.9 Hz, 1H), 1.82 (s, 9H), 1.54 (s, 7H), 1.45 (s, 9H), 1.39 (s, 9H); ¹³C DEPT NMR (151 MHz, CD₂Cl₂) δ 155.9, 155.4, 154.1, 152.0, 151.1, 149.0, 148.7, 128.3, 127.9, 122.5, 122.2, 121.1, 120.8, 120.4, 117.7, 117.6, 116.9, 116.3, 113.8, 112.1, 111.6, 108.3, 36.5, 35.5, 35.3, 35.0, 31.7, 31.6, 31.3, 31.2; HRMS (ES m/z): [M]⁺ calc. for C₃₈H₄₄O₂, 532.3336 found: 523.3370; FTIR (ATR) ν (cm⁻¹): 2955, 2903, 2866, 1728, 1627, 1618, 1570, 1518, 1462, 1425, 1393, 1362, 1308, 1261, 1236, 1227, 1207, 1167, 1121, 1084, 1063, 1026, 926, 866, 808, 763, 736, 675, 657, 601, 547, 505, 459, 414. UV/Vis (C₆H₆): λ_{\max} (ϵ)=435 (7702), 410 (9004), 389 (8224), 364 (5985), 344 (4332), 326 (3902), 310 (2662).

2,6,9,13-Tetra-*tert*-butylnaphtho[2,1-b:6,5-b']bisbenzofuran (^{1,5}fur₂): After purification by HPLC (13.6 mg injected), 2.1 mg (0.004 mmol, 3%) of the title molecule was obtained as a white solid. ¹H NMR (300 MHz, CDCl₃) δ 8.49 (s, 2H, H), 8.29 (d, J =8.3 Hz, 2H, H), 7.71 (d, J =1.6 Hz, 2H, H), 7.51 (dd, J =8.3, 1.7 Hz, 2H), 1.69 (s, 18H), 1.41 (s, 18H). ¹³C NMR (75 MHz, CDCl₃) δ 155.9, 152.7, 149.9, 135.8, 124.7, 122.2, 121.3, 120.8, 119.0, 118.4, 108.6, 77.5, 77.2, 77.0, 76.6, 35.2, 35.1, 31.7, 30.0. HRMS (ES m/z): [M]⁺ calc. for C₃₈H₄₄O₂, 532.3341 found: 532.3340; FTIR (ATR) ν (cm⁻¹): 2955, 2903, 2866, 1728, 1628, 1618, 1570, 1518, 1462, 1425, 1392, 1362, 1308, 1261, 1236, 1227, 1207, 1167, 1121, 1084, 1063, 1026, 926, 866, 808, 764, 737, 675, 658, 602, 548, 505, 459, 415. UV/Vis (C₆H₆): λ_{\max} (ϵ) 363 (8300), 347 (6300), 333 (10200), 318 (5600), 259 nm (dm³mol⁻¹cm⁻¹16600).

Crystallographic data

Deposition numbers 2105365 (for ^{1,4}pyr₂) and 2105364 (for ^{1,5}Fur₂) contain the supplementary crystallographic data for this paper. These data are provided free of charge by the joint Cambridge Crystallographic Data Centre and Fachinformationszentrum Karlsruhe Access Structures service www.ccdc.cam.ac.uk/structures.

Acknowledgements

The Authors would like to thank the EU MC-RISE "INFUSION" project (Project ID: 734834), and the H2020-RIA Decochrom project (Project ID: 760973) for financial support as well as Cardiff University, and the University of Vienna. Jack Fletcher-Charles thanks the EPSRC, in particular, for financial sponsorship of his doctoral fellowship. The Vienna Scientific Cluster is acknowledged for generous allocation of computer resources.

Conflict of Interest

The authors declare no conflict of interest.

Keywords: Cyclic voltammetry · Electrochromism · Electrochromic devices · Optoelectronics · Oxygen heterocycles

- [1] P. Andersson, R. Forchheimer, P. Tehrani, M. Berggren, *Adv. Funct. Mater.* **2007**, *17*, 3074–3082.
- [2] S. Arman, *J. New Mater. Electrochem. Syst.* **2001**, *4*, 173–179.
- [3] V. Jain, *Nanomater. Energy* **2013**, *2*, 60–63.
- [4] R. J. Mortimer, A. L. Dyer, J. R. Reynolds, *Displays* **2006**, *27*, 2–18.
- [5] R. L. Peiris, S. Nanayakkara, in *Proceedings of the 26th Australian Computer-Human Interaction Conference on Designing Futures: The Future of Design*, Association For Computing Machinery, Sydney, New South Wales, Australia, **2014**, pp. 498–504.
- [6] C. G. Granqvist, İ. Bayrak Pehlivan, G. A. Niklasson, *Surf. Coat. Technol.* **2017**, DOI 10.1016/j.surfcoat.2017.08.006.
- [7] M. Casini, *Renewable Energy* **2018**, *119*, 923–934.
- [8] W. Cheng, M. Moreno-Gonzalez, K. Hu, C. Krzyszkowski, D. J. Dvorak, D. M. Weekes, B. Tam, C. P. Berlinguette, *iScience* **2018**, *10*, 80–86.
- [9] P. S. Lee, G. Cai, A. L.-S. Eh, P. Darmawan, in *Nanomaterials for 2D and 3D Printing*, John Wiley & Sons, Ltd, **2017**, pp. 317–339.
- [10] D. V. Varaprasad, I. A. McCabe, H. Habibi, N. R. Lynam, M. Zhao, C. A. Dornan, *Electrochromic Mirrors and Devices*, **1998**, US5724187A.
- [11] P. Jarusriboonchai, E. Harjuniemi, H. Müller, A. Colley, J. Häkkinä, in *Proceedings of the 23rd International Symposium on Wearable Computers*, Association For Computing Machinery, London, United Kingdom, **2019**, pp. 274–278.
- [12] J. Häkkinä, V. Helander, D. Jamoido, A. Colley, in *Proceedings of the 2018 ACM International Joint Conference and 2018 International Symposium on Pervasive and Ubiquitous Computing and Wearable Computers*, Association For Computing Machinery, Singapore, Singapore, **2018**, pp. 734–737.
- [13] A. Colley, M. Pakanen, S. Koskinen, K. Mikkonen, J. Häkkinä, in *Proceedings of the 7th Augmented Human International Conference 2016*, Association For Computing Machinery, Geneva, Switzerland, **2016**, pp. 1–8.
- [14] A. Colley, P. W. Woźniak, F. Kiss, J. Häkkinä, in *Proceedings of the 10th Nordic Conference on Human-Computer Interaction*, Association For Computing Machinery, Oslo, Norway, **2018**, pp. 39–46.
- [15] A. Kraft, *ChemTexts* **2018**, *5*, 1.
- [16] C. G. Granqvist, *Sol. Energy Mater. Sol. Cells* **2012**, *99*, 1–13.
- [17] S. K. Deb, *Appl. Opt.*, **AO 1969**, *8*, 192–195.
- [18] S. K. Deb, *Philos. Mag.* **1973**, *27*, 801–822.
- [19] D. Gogova, A. Iossifova, T. Ivanova, Z. Dimitrova, K. Gesheva, *J. Cryst. Growth* **1999**, *198–199*, 1230–1234.
- [20] K. H. Lee, Y. K. Fang, W. J. Lee, J. J. Ho, K. H. Chen, K. C. Liao, *Sens. Actuators B* **2000**, *69*, 96–99.
- [21] E. Avendaño, A. Azens, G. A. Niklasson, C. G. Granqvist, *Sol. Energy Mater. Sol. Cells* **2004**, *84*, 337–350.
- [22] M. K. Carpenter, R. S. Conell, D. A. Corrigan, *Sol. Energy Mater.* **1987**, *16*, 333–346.
- [23] W. Estrada, A. M. Andersson, C. G. Granqvist, *J. Appl. Phys.* **1988**, *64*, 3678–3683.
- [24] C. M. Lampert, T. R. Omstead, P. C. Yu, *Sol. Energy Mater.* **1986**, *14*, 161–174.
- [25] M. Ishizaki, K. Kanaizuka, M. Abe, Y. Hoshi, M. Sakamoto, T. Kawamoto, H. Tanaka, M. Kurihara, *Green Chem.* **2012**, *14*, 1537–1544.
- [26] K. Lee, A.-Y. Kim, J. Kee Lee, *Sol. Energy Mater. Sol. Cells* **2015**, *139*, 44–50.
- [27] J. Qian, D. Ma, Z. Xu, D. Li, J. Wang, *Sol. Energy Mater. Sol. Cells* **2018**, *177*, 9–14.
- [28] R. J. Mortimer, D. R. Rosseinsky, P. M. S. Monk, *Electrochromic Materials and Devices*, John Wiley & Sons, Incorporated, Berlin, GERMANY, **2015**.
- [29] X. Cao, H. Chen, X. Gu, B. Liu, W. Wang, Y. Cao, F. Wu, C. Zhou, *ACS Nano* **2014**, *8*, 12769–12776.
- [30] D. S. Choi, S. H. Han, H. Kim, S. H. Kang, Y. Kim, C.-M. Yang, T. Y. Kim, D. H. Yoon, W. S. Yang, *Nanotechnology* **2014**, *25*, 395702.
- [31] S. M. F. Cruz, L. A. Rocha, J. C. Viana, *Flexible Electronics* **2018**, DOI 10.5772/intechopen.76161.
- [32] J. Jensen, F. C. Krebs, *Adv. Mater.* **2014**, *26*, 7231–7234.
- [33] E. O. Polat, O. Balci, C. Kocabas, *Sci. Rep.* **2014**, *4*, 1–9.
- [34] R. Singh, J. Tharion, S. Murugan, A. Kumar, *ACS Appl. Mater. Interfaces* **2017**, *9*, 19427–19435.
- [35] Z. Xu, W. Li, J. Huang, Q. Liu, X. Guo, W. Guo, X. Liu, *J. Mater. Chem. A* **2018**, *6*, 19584–19589.
- [36] V. Beedasy, P. J. Smith, *Materials* **2020**, *13*, 704.
- [37] M. Pietsch, T. Rödlmeier, S. Schliske, J. Zimmermann, C. Romero-Nieto, G. Hernandez-Sosa, *J. Mater. Chem. C* **2019**, *7*, 7121–7127.
- [38] J. A. Kerszulis, K. E. Johnson, M. Kuepfert, D. Khoshabo, A. L. Dyer, J. R. Reynolds, *J. Mater. Chem. C* **2015**, *3*, 3211–3218.
- [39] L. Beverina, G. A. Pagani, M. Sassi, *Chem. Commun.* **2014**, *50*, 5413–5430.
- [40] K. Cao, D. E. Shen, A. M. Österholm, J. A. Kerszulis, J. R. Reynolds, *Macromolecules* **2016**, *49*, 8498–8507.
- [41] P. Camurlu, E. Şahmetlioğlu, E. Şahin, İ. M. Akhmedov, C. Tanyeli, L. Toppare, *Thin Solid Films* **2008**, *516*, 4139–4144.
- [42] J. A. Kerszulis, R. H. Bulloch, N. B. Teran, R. M. W. Wolfe, J. R. Reynolds, *Macromolecules* **2016**, *49*, 6350–6359.
- [43] C. K. Lo, D. E. Shen, J. R. Reynolds, *Macromolecules* **2019**, *52*, 6773–6779.
- [44] P. M. S. Monk, R. J. Mortimer, D. R. Rosseinsky, *Electrochromism: Fundamentals and Applications*, John Wiley & Sons, **2007**.
- [45] R. J. Mortimer, *Electrochim. Acta* **1999**, *44*, 2971–2981.
- [46] L. Jia, M. Yuguo, P. Jian, S. Yanlin, *Curr. Phys. Chem.* **2011**, *1*, 216–231.
- [47] P. M. Beaujuge, J. R. Reynolds, *Chem. Rev.* **2010**, *110*, 268–320.
- [48] T. Abidin, Q. Zhang, K.-L. Wang, D.-J. Liaw, *Polymer* **2014**, *55*, 5293–5304.
- [49] L. Beverina, G. A. Pagani, M. Sassi, *Chem. Commun.* **2014**, *50*, 5413–5430.
- [50] G. Kossmehl, G. Engelmann, in *Handbook of Oligo- and Polythiophenes*, John Wiley & Sons, Ltd, **1998**, pp. 491–524.
- [51] K. Krishnamoorthy, A. V. Ambade, M. Kanungo, A. Q. Contractor, A. Kumar, *J. Mater. Chem.* **2001**, *11*, 2909–2911.
- [52] K. Krishnamoorthy, M. Kanungo, A. Q. Contractor, A. Kumar, *Synth. Met.* **2001**, *124*, 471–475.
- [53] K. Krishnamoorthy, A. V. Ambade, S. P. Mishra, M. Kanungo, A. Q. Contractor, A. Kumar, *Polymer* **2002**, *43*, 6465–6470.
- [54] T. Dey, M. A. Invernale, Y. Ding, Z. Buyukmumcu, G. A. Sotzing, *Macromolecules* **2011**, *44*, 2415–2417.
- [55] M. A. Ochieng, J. F. Ponder, J. R. Reynolds, *Polym. Chem.* **2020**, *11*, 2173–2181.
- [56] T. Kawata, M. Yamamoto, M. Yamana, M. Tajima, T. Nakano, *Jpn. J. Appl. Phys.* **1975**, *14*, 725.
- [57] F. G. K. Baucke, *Sol. Energy Mater.* **1987**, *16*, 67–77.
- [58] K. W. Shah, S.-X. Wang, D. X. Y. Soo, J. Xu, *Polymer* **2019**, *11*, 1839.
- [59] L. Striepe, T. Baumgartner, *Chem. Eur. J.* **2017**, *23*, 16924–16940.
- [60] Y. Alesanco, A. Viñuales, G. Cabañero, J. Rodriguez, R. Tena-Zaera, *ACS Appl. Mater. Interfaces* **2016**, *8*, 29619–29627.
- [61] J. Ding, C. Zheng, L. Wang, C. Lu, B. Zhang, Y. Chen, M. Li, G. Zhai, X. Zhuang, *J. Mater. Chem. A* **2019**, *7*, 23337–23360.
- [62] K.-C. Ho, H.-C. Lu, H.-F. Yu, in *Electrochromic Smart Materials*, **2018**, pp. 372–405.

- [63] M. Li, Y. Wei, J. Zheng, D. Zhu, C. Xu, *Org. Electron.* **2014**, *15*, 428–434.
- [64] G. J. Stec, A. Lauchner, Y. Cui, P. Nordlander, N. J. Halas, *ACS Nano* **2017**, *11*, 3254–3261.
- [65] A. Lauchner, A. E. Schlather, A. Manjavacas, Y. Cui, M. J. McClain, G. J. Stec, F. J. García de Abajo, P. Nordlander, N. J. Halas, *Nano Lett.* **2015**, *15*, 6208–6214.
- [66] A. Rossignon, D. Bonifazi, *Synthesis* **2019**, *51*, 3588–3599.
- [67] H. Tsuji, E. Nakamura, *Acc. Chem. Res.* **2017**, *50*, 396–406.
- [68] C.-C. Wu, W.-Y. Hung, T.-L. Liu, L.-Z. Zhang, T.-Y. Luh, *J. Appl. Phys.* **2003**, *93*, 5465–5471.
- [69] H. Tsuji, C. Mitsui, L. Ilies, Y. Sato, E. Nakamura, *J. Am. Chem. Soc.* **2007**, *129*, 11902–11903.
- [70] H. Tsuji, C. Mitsui, Y. Sato, E. Nakamura, *Adv. Mater.* **2009**, *21*, 3776–3779.
- [71] C. Mitsui, H. Tsuji, Y. Sato, E. Nakamura, *Chem. Asian J.* **2012**, *7*, 1443–1450.
- [72] L. Wojcik, F. Michaud, S. Gauthier, N. Cabon, P. Le Poul, F. Gloaguen, N. Le Poul, *J. Org. Chem.* **2017**, *82*, 12395–12405.
- [73] O. Anamimoghdam, M. D. Symes, D.-L. Long, S. Sproules, L. Cronin, G. Bucher, *J. Am. Chem. Soc.* **2015**, *137*, 14944–14951.
- [74] A. Jha, P.-J. J. Huang, *J. Heterocycl. Chem.* **2009**, *46*, 1098–1106.
- [75] J. J. Vaquero, A. M. Cuadro, B. Herradón, in *Modern Heterocyclic Chemistry*, John Wiley & Sons, Ltd, n.d., pp. 1865–1988.
- [76] S. Yamaguchi, N. Tsuchida, M. Miyazawa, Y. Hirai, *J. Org. Chem.* **2005**, *70*, 7505–7511.
- [77] N. Kobayashi, M. Sasaki, K. Nomoto, *Chem. Mater.* **2009**, *21*, 552–556.
- [78] R. Pummerer, E. Prell, A. Rieche, *Ber. Dtsch. Chem. Ges. A&B* **1926**, *59*, 2159–2161.
- [79] A. Dettling, A. Rieker, B. Speiser, *Tetrahedron Lett.* **1988**, *29*, 4533–4534.
- [80] G. Frenking, A. Rieker, J. Salbeck, B. Speiser, *Z. Naturforsch. B* **1996**, *51*, 377–380.
- [81] L. Đorđević, C. Valentini, N. Demitri, C. Mézière, M. Allain, M. Sallé, A. Folli, D. Murphy, S. Mañas-Valero, E. Coronado, D. Bonifazi, *Angew. Chem. Int. Ed.* **2020**, *59*, 4106–4114; *Angew. Chem.* **2020**, *132*, 4135–4143.
- [82] T. Miletic, A. Fermi, I. Orfanos, A. Avramopoulos, F. De Leo, N. Demitri, G. Bergamini, P. Ceroni, M. G. Papadopoulos, S. Couris, D. Bonifazi, *Chem. Eur. J.* **2017**, *23*, 2363–2378.
- [83] D. Stassen, N. Demitri, D. Bonifazi, *Angew. Chem. Int. Ed.* **2016**, *128*, 6051–6055.
- [84] A. Berezin, N. Biot, T. Battisti, D. Bonifazi, *Angew. Chem. Int. Ed.* **2018**, *57*, 8942–8946; *Angew. Chem.* **2018**, *130*, 9080–9084.
- [85] A. Scitutto, A. Berezin, M. Lo Cicero, T. Miletic, A. Stopin, D. Bonifazi, *J. Org. Chem.* **2018**, *83*, 13787–13798.
- [86] A. Scitutto, A. Fermi, A. Folli, T. Battisti, J. M. Beames, D. M. Murphy, D. Bonifazi, *Chem. Eur. J.* **2018**, *24*, 4382–4389.
- [87] L. Đorđević, D. Milano, N. Demitri, D. Bonifazi, *Org. Lett.* **2020**, *22*, 4283–4288.
- [88] W. Guo, E. Faggi, R. M. Sebastián, A. Vallibera, R. Pleixats, A. Shafir, *J. Org. Chem.* **2013**, *78*, 8169–8175.
- [89] R. G. Harvey, J. Pataki, C. Cortez, P. Di Raddo, C. X. Yang, *J. Org. Chem.* **1991**, *56*, 1210–1217.
- [90] A. D. Becke, *J. Chem. Phys.* **1993**, *98*, 5648–5652.
- [91] C. Lee, W. Yang, R. G. Parr, *Phys. Rev. B* **1988**, *37*, 785–789.
- [92] R. Krishnan, J. S. Binkley, R. Seeger, J. A. Pople, *J. Chem. Phys.* **1980**, *72*, 650–654.
- [93] J. Tomasi, B. Mennucci, R. Cammi, *Chem. Rev.* **2005**, *105*, 2999–3094.
- [94] H. Konishi, K. Aritomi, T. Okano, J. Kiji, *Bull. Chem. Soc. Jpn.* **1989**, *62*, 591–593.

Manuscript received: September 19, 2021
Revised manuscript received: November 4, 2021
Accepted manuscript online: November 8, 2021